



Hydrochemical and stable isotope data of water in karst aquifers during normal flow in South Africa

Naziha Mokadem¹ · Rainier Dennis¹ · Ingrid Dennis¹

Received: 27 September 2020 / Accepted: 28 July 2021 / Published online: 9 August 2021
© The Author(s), under exclusive licence to Springer-Verlag GmbH Germany, part of Springer Nature 2021

Abstract

The dolomite aquifer in Witwatersrand is one of the most important water resources in South Africa. The present paper aims to evaluate the hydrochemical and isotope ($\delta^2\text{H}$ and $\delta^{18}\text{O}$) signature of water ($n = 36$) (groundwaters, surface waters, dams, springs, canal, cave and pipeline) of the Wonderfontein spruit (WFS). These samples were analysed for the first time in the Centre for Water Sciences and Management (South Africa). The dominant anions are SO_4^{2-} and Cl^- , while the dominant cations are Ca^{2+} followed by Mg^+ , Na^+ and K^+ . A Piper diagram showed that there are two principal hydrochemical facies (1) Ca–Mg–Cl– SO_4 ; (2) Ca–Mg– HCO_3 in the study area. Bivariate plots revealed that the main hydrogeochemical processes influencing the water are water–rock interaction, mineral precipitation/dissolution, ions exchange and anthropogenic activities. The local meteoric water line (LMWL) was plotted for the first time for the WFS catchment based on precipitation data during six periods (November 2018 until June 2019) with the following equation $\delta^2\text{H} = 7.39 * \delta^{18}\text{O} + 7.9\text{‰}$ ($R^2 = 0.85$). The results of stable isotopes ($\delta^2\text{H}$ and $\delta^{18}\text{O}$) indicated that the water points from local precipitation and recent water, and the groundwater recharge is influenced by rapid infiltration river flow and return irrigation flow.

Keywords Karst system · Hydrochemical · Stable isotope · Local meteoric water line (LMWL) · South Africa

Introduction

Owing to climate change, urban expansion and population growth, the equilibrium between water supply and human demand (domestic, industrial and agriculture) have increased over the last decades in the world. This problem of water scarcity is greatly affecting the arid and semi-arid areas in Africa (Allan 2002; Connor et al. 2017; Morsy et al. 2018). South Africa (SA) is one of the countries in Africa that have several mineral deposits like gold, diamonds, coal, uranium and platinum. Conversely, SA suffers from a scarcity of water resources, which is mainly caused by pollution of natural water of rivers, streams, springs, dams by anthropogenic

activities that include, industrial, mining activities, farming, etc.

The karst aquifers situated in the Far West Rand (FWR) goldfield of the Witwatersrand Basin and in WFS catchment represent a significant groundwater resource in SA (Schrader and Winde 2015). The groundwater management in the deep-level gold mines below the dolomites is in a disadvantageous state due to the morpho-structural context development and the considerable volume of groundwater that changes the flowing regime into the mine voids, making the exploitation of gold both risky and expensive (Hodgson et al. 2001; Schrader and Winde 2015).

Therefore, the mining infrastructure, such as tunnels, haulages, waste rock dumps, tailings, storage facilities, evaporation dams and pipelines, plays an important role in changing groundwater flow and recharge conditions. Mining-related impacts in the FWR include the dewatering of four groundwater compartments namely Venterspost, Oberholzer, Bank and Gembokfontein which results in a drop in the water table (> 300 m in some places) and several boreholes in farming areas and karst springs dry up. Water circulation is discharged via canals and pipelines outside the boundaries

✉ Naziha Mokadem
mokademnaziha86@gmail.com; nazouhmoka@gmail.com

Rainier Dennis
rainier.dennis@nwu.ac.za

Ingrid Dennis
ingrid.dennis@nwu.ac.za

¹ Centre for Water Sciences and Management, North-West University, 11 Hoffman Street, Potchefstroom 2531, South Africa

of the dewatered compartments (Swart et al. 2003a, b; Coetzee et al. 2006a, b; Schrader and Winde 2015).

Mining activities in WFS have also impacted negatively on both the quantity and quality of ground and surface water. Generally, the groundwater quality is mostly influenced by many factors such as the intermixing of water, rock–water interactions, climatic conditions, geological formations, dissolution and precipitation, oxidation–reduction, recharge and discharge, residence time, the transformation of organic matter and various anthropogenic activities (Faure 1998; Barbécot et al. 2000; Belkhiri et al. 2010; Ledesma-Ruiz et al. 2015; Al-Khashman 2008; Sharif et al. 2008; Pazand and Fereidoni Sarvestani 2013; Pazand 2014; Yang et al. 2016; Hamed 2015; Mokadem et al. 2016). To study these processes influencing groundwater quality, a thorough hydrogeochemical investigation is needed in the WFS catchment. In that context, the application of stable isotopes of water ($\delta^{18}\text{O}$ and $\delta^2\text{H}$) is an excellent way to fingerprint and evaluate various hydrological processes in the Witwatersrand Basin, such as identification of recharge and discharge areas, mixing process, qualitative groundwater pathways, salinization of groundwater, evaporation and condensation, surface air temperature and recharge altitude (Craig 1961; Clark and Fritz 1997; Dotsika et al. 2010; Abyie et al. 2011).

A large amount of research related to the WFS catchment has been published (IWQS 1999; Wade et al. 2002; Coetzee et al. 2002; Swart et al. 2003a, b; Coetzee et al. 2006a, b; Schrader and Winde 2015; Durand 2012; Brink 1979; Bredenkamp 1993; Enslin and Kriel 1967; Fleisher 1981; Foster 1988; Wolmarans 1984).

The aims of the present study are to: (1) provide a better understanding of the evolution of water, (2) determine the hydrochemical facies, rock–water interaction and the role of anthropogenic activities, (3) identify recharge–discharge areas and to generate a Local Meteoric Water Line (LMWL) (not generated before) using an integrated hydrochemical and isotopic approaches.

Site description

The name Wonderfonteinspruit means “Wonderful-fountain-stream” defining the ample volumes of dolomitic groundwater that once supplied the stream by means of karst springs (eyes). The WFS catchment, also known as the WFS Valley (De Kock 1967), is located in the historic mining district of the Witwatersrand region. The study area is famous in SA for its gold mines. It is situated between longitude 27°0'0"–27°60'0" east and latitude 26°0'0"–26°40'0" south with a topography ranging from 1322 to 1839 m (m) above sea level (a.s.l.) (Fig. 1a–c).

The WFS river runs over 90 km from Johannesburg, past the towns of Krugersdorp, Bekkersdal, Carletonville and Khutsong and flows into the Mooi River near Potchefstroom.

The region has a warm sub-humid climate with summer rainfall (November–March) and dry winters (June–August). The average annual rainfall is approximately 700 mm per annum. The average evaporation rate for the area is in the order of 1560 mm (De Klerk 2018).

Geological and hydrogeological setting

The Wonderfonteinspruit valley is partially concentrated at two major goldfields, namely (1) The West Rand and (2) The FWR. The goldfields of the West Rand are situated approximately 50 km south–west of Johannesburg (Fig. 2a, b). These goldfields are located in the headwaters of the non-dolomitic portion of the WFS and includes active gold mines.

The FWR goldfields host some of the first gold mines in South Africa, which are located in the upper area of the lower WFS (downstream of Donaldson Dam). According to Cole (1998), the FWR was the richest mined goldfield in the Witwatersrand Basin. This Goldfield contains the following: ‘West Wits Line’ regrouping gold mines around the town of Westonaria (Libanon, Venterspost, Western Area, Kloof, South Deep) and the Carletonville mining area close to the city of Merafong comprising mines (Doornfontein, Elandsrand, Blyvooruitzicht, West and East Driefontein, Deelkraal and Western Deep Levels) (Robb and Robb 1998).

The Witwatersrand supergroup acquired its name from a description of the auriferous outcrop on the Witwatersrand. The Witwatersrand supergroup (approximately 8000 m thick) is subdivided into two major groups namely the West Rand Group and Central Rand Group (Fig. 2a, b). The West Rand Group is characterized by the presence of some gold and a lithology including shale and quartzite. This group contains three formations from bottom to top, namely the Hospital hill subgroup, the Government Reef subgroup and Jeppetown subgroup (Fig. 2a, b). The Central Rand Group is in turn divided into two units: Johannesburg Subgroup and the Turffontein Subgroup. The first strata (Johannesburg Subgroup) has the richest, most exploited gold deposits in the Witwatersrand Basin. These subgroups in the Central Rand Group include the reefs mined in the West Rand and FWR goldfields such as Leader Reef, Middelvlei Reef, the Elsburg Reef and Composite Reef (McCarthy and Rubidge 2005; Viljoen and Reimold 2002). Approximately 8 m thick of igneous rocks known as Ventersdorp Contact Reef is found between the upper sections of the Witwatersrand sediments and the base of the Ventersdorp Supergroup (Brink 1979; Els 1987, 2000). The latter (approximately 600 m thick) includes three groups namely, the Klipriviersberg, Platberg, Priel Groups. The Transvaal Supergroup was deposited above the Ventersdorp Supergroup. The bottom layer of The Transvaal Supergroup known as the Black

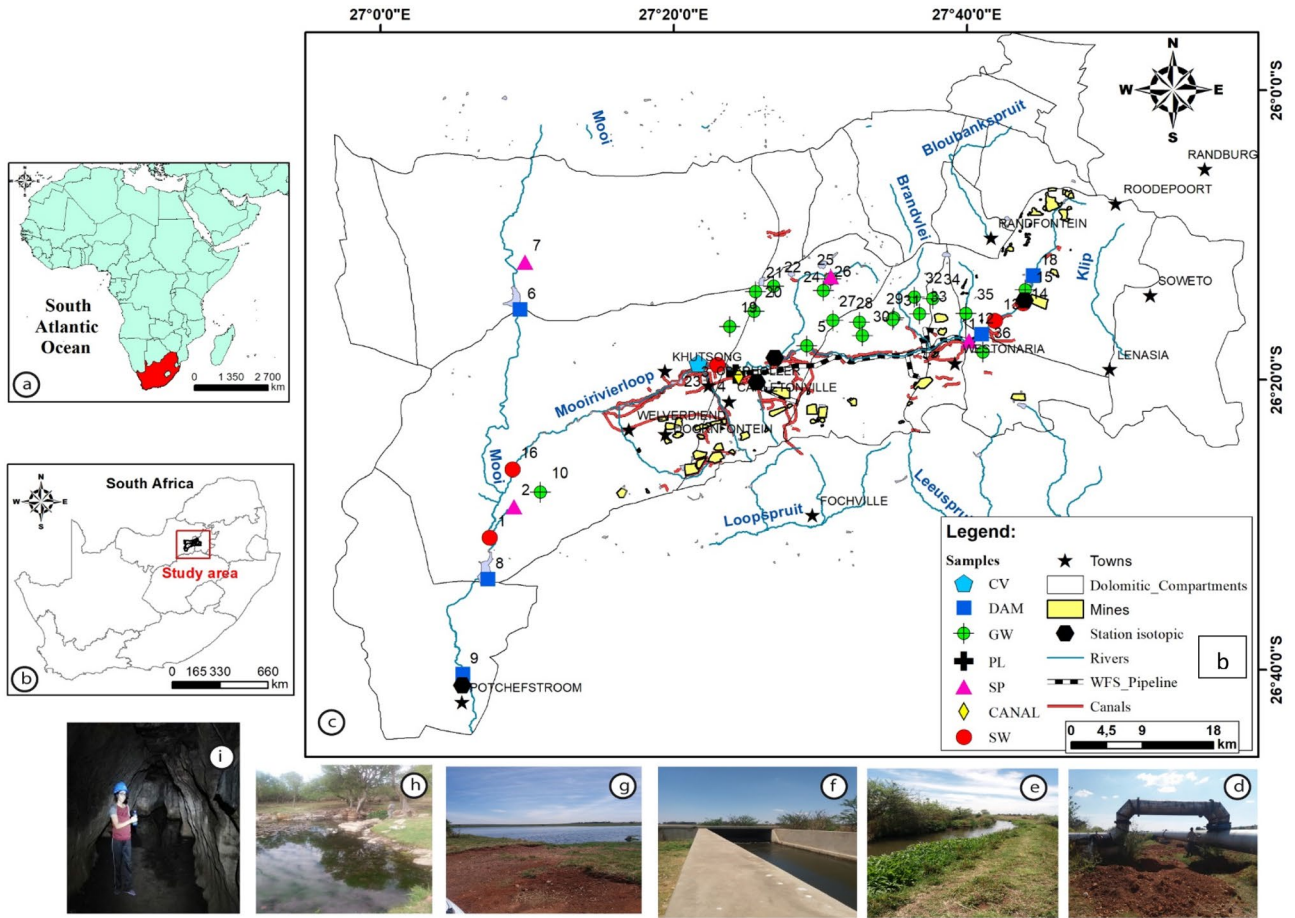


Fig. 1 Location (a, b) and sampling (c) map of the study area: d pipeline; e Wonderfonteinspruit; f canal; g dam; h spring; i cave

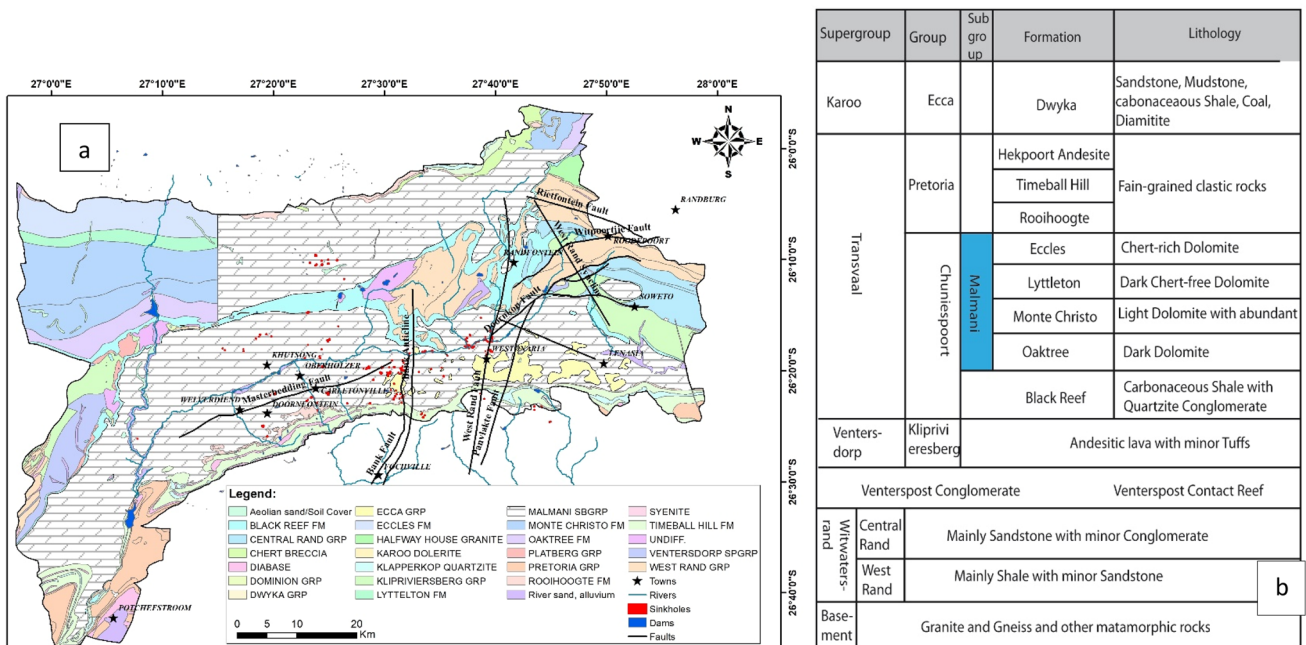


Fig. 2 a Geological map, b lithostratigraphic column of the study area

Reef, is approximately 10 m thick. The latter contains limited deposits of gold and is the unique reef in the study area exploited by opencast mining. The Transvaal Supergroup is subdivided into two groups (a) Chunispoort (b) Pretoria. The former contains dolomite of the Malmani Subgroup. This Subgroup contains four formations as shown in Fig. 2b. These formations contain chert. The highly chert-rich dolomite is located in Eccles Formation and Monte Christo Formation; these cover the majority of the dolomite outcrops in the region. This is unlike the Oak Tree and Lyttelton Formations which are chert-poor. Therefore, the chert-rich formations form the main aquifers (McCarthy and Rubidge 2005; Eriksson and Reczko 1995). This dolomite is overlain by the Pretoria Group.

The area is characterized by a series of lineaments representing dolerite dykes and faults. The dykes are mainly semi- or impermeable barriers. The natural boundaries divide the dolomites into many compartments, including from east to west the Zuurbekom, Gemsbokfontein, Venterpost, Bank, Oberholzer and Boskop-Turffontein Compartments. The permeability of these dolomites compartments is mostly due to secondary fissures such as joints and faults which provide the easy circulation of groundwater and controlling its flow direction in the weathered regions. The four main lineaments in the area (Fig. 2a) are as follows: West Rand (NNW–SSE), Transkaroo (NE–SW), Bank (NW–SE) and Witpoortjie (NNE–SSW) (Brink 1979). The Bank and Witpoortjie faults generally penetrate through the dolomites and are filled with clayey residual material. The Bank fault separates the goldfield into the FWR goldfield and the Carletonville goldfield (Robb and Robb 1998). These two lineaments form conduits for groundwater flow. On the other side, Libanon and Doornfontein are the dry mines in the area due to the mylonitic of Trans-Karoo and West Rand faults.

The karstification of the region results in many large feature both on the surface and beneath. In WFS valley many sizes and type of Karst forms are developed such as flute, small feature, runnels, lapiez, sinkholes. The principal result of the karstification is dissolving of the carbon rocks by carbonic acid, owned by reaction of the carbon dioxide with water. The weakly-acidic groundwater circulating along tension fractures, faults and joints in the dolomitic succession causes leaching of the carbonate minerals. However, gypsum is dissolved by sulfuric acid, which is formed by reaction of the oxygen with H_2S . So, the surface water rich with oxygen seep into deep anoxic karst systems, it causes oxygen to react with sulphide present in the system (H_2S) to form sulfuric acid (H_2SO_4). The process of karstification is characterized by: chemical dissolution of the soluble element of the carbonate rock, simultaneous removal of the dissolved species and mechanical erosion of the undissolved particles and the creation of open voids (Dubois et al. 2014; Sissakian et al. 2016).

In WFS valley are prone to sudden, catastrophic collapse which can lead to death, injury or structural damage. These phenomena are known as sinkholes and occur in areas underlain by dolomite rock in the study area (Buttrick et al. 2001). Jennings et al. (1965) and Brink (1979) proved that sinkholes can form owing to concentrated ingress of water or dewatering of compartment (Fig. 3). However, (i) the huge active subsurface erosion caused by concentrated penetration of water will result in downwards transportation of materials into the nearest cavity, (ii) the mechanism of triggering leads to the breaching of the last arch. Particularly in the case of small sinkholes, the cross-section resembles a narrow opening at the surface, a shape that may be maintained for some time and (iii) the lowering of the water table

Fig. 3 Example of sinkholes in study area



perturbs the equilibrium and active subsurface erosion may be accelerated. Buoyant support within the overburden is also removed, leading to compression of the wad which may lead to collapse. Therefore, the natural process of sinkholes formation in the study is area owing to the accelerating groundwater level drawdown known as ‘dewatering’. According to Brink (1979) in the Far West Rand sinkholes set off by dewatering could achieve depths of 50 m and diameters of 125 m, while sinkholes triggered by ingress that are mostly smaller.

However, the mining activities in the WFS Valley have had many negative impacts on groundwater level, storage, quantity and quality, which caused the drying-up of springs (e.g. Venterspost spring, Bank spring and Oberholzer spring). The resultant formation of sinkholes continues today (Fig. 2a). Furthermore, all these problems are considered to be repercussions of an official policy to deliberately dewater which was implemented for the Venterspost and Oberholzer Compartments in 1964, Bank Compartment in 1969 and Gembokfontein Compartment in the late 1980s (Enslin and Kriel 1967). The dewatering of compartments has an impact on pumping rates (Wolmarans 1984). For instance, in September 1955 to April 1973, with the dewatering of the Oberholzer Compartment, the pumping rates decreased from 170 to 50 ml/day (Hodgson et al. 2001).

Hence, to avoid recirculation of water in the study area, water pumped from fissures, sinkholes and underground mine workings is discharged outside the boundaries of the dewatered dolomitic compartments in pipelines and canals. A large volume of the pumped water is discharged into the WFS and to adjacent catchments. The pipelines in WFS valley are approximately nearly 30 km in length (Fig. 1c).

The study area contains several dams, the most important among them the Donaldson Dam which has an impact on the WFS. Here, the river flow circulates through a pipeline over dolomites (Fig. 1c). The dam transports the water over the dolomitic groundwater compartments (with storage about 1000 ml) to where it discharges close to Carletonville. The diversion of the river from its natural channel has been designed to allow deep gold mining to proceed below the outcropping dolomite.

In this area, several types of research have been published which involved calculating the dolomitic compartments recharge in the WFS (Wolmarans 1984; Bredenkamp 1993; Fleisher 1981; Foster 1988; Enslin and Kriel 1967) indicated that average groundwater recharge for each compartment is 14.7% (Zuurbekom compartment), 13.1% (Gembokfontein compartment), 27.5% (Venterspost compartment), 16.2% (Bank compartment), 11.6% (Oberholzer compartment) and 5.6% (Boskop-Turffontein).

Materials and methods

Sampling and laboratory analyses

Water points were collected during normal flow in February 2019 from 19 boreholes, 5 surface watersources, 5 Dams (namely Klerkskraal Dam, Boskop Dam, Potchefstroom Dam, Donaldson Dam and Luipaardsvlei Dam), 4 springs (named Gerhard Minnebron, Bovenste Oog, Gembokfontein Spring and ROD01), 1 canal, 1 pipelines, 1 cave), a total of 36 samples within the study area for hydrochemistry and ^2H and ^{18}O analyses (Fig. 1c, e–i).

The water samples were collected in 500 ml bottles for subsequent chemical and isotopic analysis in the laboratory (Fig. 4a). All bottles were labelled with code number, ID, date of sampling and coordinates. Chemical and isotopic analyses were carried out at the Centre for Water Sciences and Management of the North–West University of Potchefstroom (South Africa).

The pH was measured using a pH metre 510 (Fig. 4b), the electrical conductivity (EC) was measured using a multi-parameter WTW model 3210 (Fig. 4c) and alkalinity (Alk) was determined with a pH metre with volumetric titration using HCl to pH 4.5; 4.2 and 8.2 (Fig. 4d). The chemical analyses of the anion components (Cl^- , SO_4^{2-} , Alk, NO_3^-) were performed using Metrohm ion chromatography, 761 compact IC model (Fig. 4e), with a precision of ± 0.001 mg/l and for the cation components (Na^+ , Mg^+ , K^+ , Ca^+) were analysed using a Metrohm ion chromatography, ICP-MS 7500 series (Fig. 4f). Samples were filtered before being analysed in chromatography line.

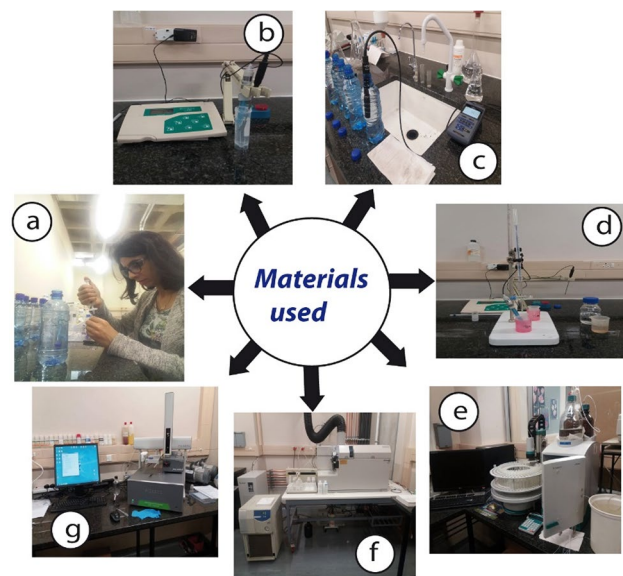


Fig. 4 Materials used

$\delta^{18}\text{O}$ and $\delta^2\text{H}$ relative to the Vienna-Standard Mean Ocean Water (RVSMOW), were determined by Picarro L2130-I Isotopic H_2O (Cavity Ring down laser spectrometer, Picarro Ltd.) (Fig. 4g). The mineral saturation indices (SI) such as dolomite calcite gypsum halite were calculated using PHREEQC[®] software (Parkhurst and Appelo 1999) (Table 1).

Results and discussion

Hydrochemical result

Hydrochemical parameters

The assessment of the geochemical analyses of the WFS includes physical parameters such as EC and pH together with major cations and anion ions. These parameters were analysed for their respective minimum, maximum, mean standard deviation and coefficient of variance of 36 water type samples (groundwater, surface water, spring, dam, canal, pipeline and cave) are listed in Table 1. The $p\text{CO}_2$ in the Karst water samples varies between 0.27 and 96.94 10^{-3} atm more than $p\text{CO}_2$ of the precipitations ($10^{-3.5}$ atm) (Table 1). Figure 5a shows a good correlation between pH and $p\text{CO}_2$, that indicates a dissolution of the carbonate (calcite and dolomite) enhanced by the acidic rainwater (Edet and Offiong 2002; Ayadi et al. 2018a, b). Most of the water samples show rapid circulation via karst conduits like faults, sinkholes and the impact of recent rainfall infiltration. Figure 5a illustrates a drop in pH caused an increase in $p\text{CO}_2$. pH result shows that most of the water samples in the region are slightly alkaline, with an average values 6.63, 7.53, 6.87, 7.7, 7.15, 7.9 and 7.11, respectively, groundwater, surface water, spring, dam, pipeline, canal, cave. Electrical conductivity (EC) is a measure of an ability to conduct current and higher EC indicates the enrichment of salts/dissolved matter in water. Electrical conductivity value in the study area ranging from 0 to 1.13 mS/cm (Fig. 5b). Most of the water types have a mean EC value (around 0.6–0.9 mS/cm) except for groundwater which has a mean value of 0.2 mS/cm. Majority of the samples have the values less than 1 mS/cm indicating rapid infiltration, recent water, regular recharge and rapid water circulation due to the high hydraulic conductivity and different residence time of the karst water within the area. These factors govern the variation in the chemical component that most influence the EC such as Mg^{2+} , SO_4^{2-} , Ca^{2+} with come from the dissolution of aquifer bedrock after each recharge event and impact of anthropogenic activities. The average concentrations abundance of major ions in the study area are as follows $\text{HCO}_3 > \text{SO}_4 > \text{Ca} > \text{Cl} > \text{Mg} > \text{Na} > \text{K}$. The average values of potassium (K^+) are 1.6, 6.2, 3.83, 7.35, 5, 2.93 and 5.83 mg/l in groundwater, surface water,

spring, dam, pipeline, canal and cave, respectively. The maximum alkalinity observed in surface waters and dams was between 210 to 285 mg/l with an average of 252 mg/l and 222.5 to 340 mg/l with an average of 263.5 mg/l, respectively. The high concentrations of calcium are located in surface water samples ranging between 50.87 and 93.29 mg/l with an average of 70.74 mg/l. Surface water and cave samples show high Cl contents with values 65.81 and 76.69 mg/l, respectively. The mean values of sulphate ions (mg/l) in groundwater, surface water, spring, dam, pipeline, canal and cave were 28.16, 201.31, 121.95, 132.5, 214.33, 293.59 and 243.63 mg/l, respectively. The average sodium value of groundwater samples is lower than the average of the rest of the other types of water samples Table 1. All types of water (groundwater, surface water, spring, dam, pipeline, canal, cave) have similar maximum Mg values, ranging from 33 to 49 mg/l. The maximum nitrate content is that of the groundwater sample and is 63.44 mg/l. Most of the maximum mean values of major (cation and anion) ions in the study area were observed in surface water. Generally, the physical and hydrochemical parameters of water samples during this period show that the majority of parameters have a high coefficient of variance (CV%) > 50% which signifies there is a spatial variation between the samples (Table 1).

Hydrochemical facies

The identification of hydrochemical facies of all types of water samples within the WFS Valley, have been analysed and plotted on the trilinear diagram Piper diagram (Piper 1944). This diagram has a rhombus and two triangles. Each one of the triangles indicates three ion percentages of concentrations and the rhombus presents the water composition according to anions and cations (Fetter 2014). Five hydrochemical facies have been identified in the study area (Fig. 6): Two main facies: (1) Ca-Mg-Cl-SO_4 (S1, S2, S3, S4, S5, S10, S11, S14, S15, S16, S17, S22, S23, S30); (2) Ca-Mg-HCO_3 (S6, S7, S8, S9, S19, S20, S21, S24, S27, S28, S29, S31, S32, S33, S34, S35) and three second groups: (3) Ca-Mg-SO_4 (S12, S13, S36); (4) Mg-HCO_3 (S6, S25, S26) and (5) Na-K-HCO_3 (S18). The first facies includes the surface water samples, canal, cave, pipeline, Gerhard Minnebron and Gemsbokfontein springs and few groundwater samples. The second facies characterizes the majority of boreholes of Malmani aquifer (Transvaal Supergroup), most of dam samples and Bovenste spring. The Ca-Mg-SO_4 type (with higher SO_4 concentration) represents samples located upstream of WFS. The Mg-HCO_3 facies belongs to samples collected from two wells and the Klerkskraal Dam. The Luipaardsvlei Dam shows Na-K-HCO_3 hydrochemical facies.

Table 1 Geochemical and isotope characteristics of the analysed samples in the study area

Type water	N	Name	pH	EC (ms/cm)	Alk (mg/l)	K (mg/l)	Ca (mg/l)	Cl (mg/l)	NO ₃ (mg/l)	SO ₄ (mg/l)	Na (mg/l)	Mg (mg/l)	¹⁸ O SMOW‰	² H SMOW‰	D SMOW‰	Calcite	Dolomite	Gyp-sum	Halite	pCO ₂ (10 ⁻³ atm)
Surface waters	1	Mooi River	7.55	0.78	255.00	1.78	71.57	38.11	4.13	138.66	27.10	42.83	-2.60	-15.66	5.16	0.27	0.67	-1.55	-7.58	7.75
	3	WFS3	7.74	0.86	210.00	4.79	64.32	47.38	7.11	239.90	52.76	38.74	-2.85	-15.36	7.46	0.30	0.71	-1.38	-7.20	4.11
	13	WFS4	7.35	0.78	245.00	10.44	93.29	65.81	12.04	381.69	100.80	25.93	-1.27	-5.54	4.61	0.08	-0.05	-1.08	-6.79	11.82
	14	WFS5	7.40	1.13	265.00	11.82	50.87	36.63	12.37	76.63	72.69	11.67	-0.84	-2.98	3.72	0.03	-0.23	-1.86	-7.16	11.39
	16	WFS2	7.63	0.84	285.00	2.44	73.69	43.27	4.44	169.69	37.77	40.48	-2.37	-13.61	5.32	0.40	0.88	-1.46	-7.38	7.20
		Min	7.35	0.78	210.00	1.78	50.87	36.63	4.13	76.63	27.10	11.67	-2.85	-15.66	3.72	0.03	-0.23	-1.86	-7.58	4.11
		Max	7.74	1.13	285.00	11.82	93.29	65.81	12.37	381.69	100.80	42.83	-0.84	-2.98	7.46	0.40	0.88	-1.08	-6.79	11.82
		Mean	7.53	0.88	252.00	6.25	70.75	46.24	8.02	201.31	58.22	31.93	-1.99	-10.63	5.25	0.22	0.40	-1.47	-7.22	8.45
		SD	0.16	0.15	27.75	4.62	15.44	11.74	4.00	116.72	29.32	13.08	0.88	5.94	1.38	0.16	0.50	0.28	0.29	3.20
		CV%	2.14	16.85	11.01	73.83	21.83	25.39	49.83	57.98	50.36	40.98	-44.41	-55.85	26.33	72.06	126.18	-19.25	-4.06	37.82
Springs	2	Gerhard Minnebron	7.12	0.84	225.00	1.62	73.99	49.26	10.71	182.22	30.46	43.40	-2.99	-16.40	7.54	-0.21	-0.30	-1.43	-7.42	18.45
	7	Bovenste eye	7.09	0.44	265.00	1.28	44.63	2.70	6.05	3.49	3.07	26.29	-4.62	-26.91	10.03	-0.28	-0.45	-3.21	-9.65	23.29
Dams	11	Gembokfontein Spring	7.87	1.10	210.00	11.60	92.24	52.60	3.58	299.68	99.70	25.38	-1.01	-4.39	3.70	0.55	0.88	-1.16	-6.88	3.04
	25	ROD01	5.40	0.10	22.50	0.82	2.95	2.58	3.07	2.43	3.79	5.91	-3.63	-20.28	8.76	-4.09	-7.53	-4.30	-9.53	96.94
		Min	5.40	0.10	22.50	0.82	2.95	2.58	3.07	2.43	3.07	5.91	-4.62	-26.91	3.70	-4.09	-7.53	-4.30	-9.65	3.04
		Max	7.87	1.10	265.00	11.60	92.24	52.60	10.71	299.68	99.70	43.40	-1.01	-4.39	10.03	0.55	0.88	-1.16	-6.88	96.94
		Mean	6.87	0.62	180.63	3.83	53.45	26.79	5.85	121.96	34.26	25.25	-3.06	-17.00	7.51	-1.01	-1.85	-2.53	-8.37	35.43
		SD	1.04	0.44	107.94	5.19	38.96	27.91	3.49	145.53	45.45	15.32	1.52	9.45	2.73	2.09	3.83	1.49	1.43	41.91
		CV%	15.20	71.23	59.76	135.51	72.89	104.21	59.63	119.33	132.69	60.70	-49.69	-55.63	36.40	-207.35	-207.19	-59.11	-17.05	118.28
		Klerkskraal Dam	7.62	0.37	225.00	1.26	22.90	2.91	0.10	3.45	3.42	29.50	-1.60	-10.99	1.80	-0.10	0.26	-3.48	-9.56	5.82
		Boskop Dam	7.42	0.80	300.00	9.59	53.51	45.60	0.61	126.83	27.31	49.07	1.20	7.38	-2.22	0.09	0.49	-1.71	-7.50	12.31
		Potchefstroom Dam	7.70	0.72	230.00	2.02	45.56	43.52	0.25	142.09	29.02	45.73	-0.42	-2.85	0.54	0.19	0.72	-1.71	-7.49	4.94
Pipeline	4	PI	7.15	0.83	205.00	5.00	60.02	43.80	8.52	214.33	54.40	33.05	-2.90	-15.58	7.61	-0.31	-0.55	-1.43	-7.22	15.69
	17	Canal	7.90	0.87	285.00	2.93	52.57	52.19	1.21	293.59	44.80	46.21	-2.81	-15.01	7.50	0.47	1.23	-1.40	-7.23	3.85
Dams	12	Donaldson Dam	8.30	1.10	222.50	11.46	92.22	52.98	2.12	298.22	98.64	25.18	-0.96	-4.16	3.56	0.98	1.75	-1.17	-6.89	1.18
	18	Luipaardsvlei Dam	7.50	0.84	340.00	12.45	47.82	43.05	2.47	91.95	70.73	10.53	-0.59	-1.31	3.41	0.20	0.09	-1.82	-7.10	11.60
Surface waters		Min	7.42	0.37	222.50	1.26	22.90	2.91	0.10	3.45	3.42	29.50	-1.60	-10.99	1.80	-0.10	0.26	-3.48	-9.56	5.82
		Max	8.30	1.10	340.00	12.45	92.22	52.98	2.47	298.22	98.64	49.07	1.20	7.38	-2.22	0.09	0.49	-1.71	-7.50	12.31
		Mean	7.71	0.77	263.50	7.36	52.40	37.61	1.11	132.51	45.82	32.00	-0.48	-2.38	1.42	0.27	0.66	-1.98	-7.71	7.17
		SD	0.35	0.26	53.55	5.32	25.12	19.80	1.10	107.10	38.19	15.76	1.04	6.59	2.38	0.41	0.65	0.88	1.07	4.71
		CV%	4.52	34.27	20.32	72.35	47.94	52.65	99.50	80.83	83.33	49.25	-218.85	-276.5	168.1	152.11	98.64	-44.34	-13.85	65.68

Table 1 (continued)

Type	N	Name	pH	EC (ms/cm)	Alk (mg/l)	K (mg/l)	Ca (mg/l)	Cl (mg/l)	NO ₃ (mg/l)	SO ₄ (mg/l)	Na (mg/l)	Mg (mg/l)	¹⁸ O SMOW‰	² H SMOW‰	D SMOW‰	Calcite	Dolomite	Gyp-sum	Halite	pCO ₂ (10 ⁻³ atm)	
Cave	23	CV	7.11	0.94	195.00	5.83	62.31	76.69	7.68	243.63	62.89	39.23	-2.45	-12.75	6.87	-0.38	-0.61	-1.39	-6.92	16.36	
Groundwaters	5	BH1	6.04	0.25	55.00	2.68	13.48	10.85	63.44	8.65	8.39	11.04	-4.13	-22.87	10.15	-2.47	-4.67	-3.20	-8.59	54.28	
	10	JW01	7.22	0.80	270.00	1.61	69.27	43.14	8.94	154.51	29.06	41.60	-2.94	-15.95	7.54	-0.05	0.02	-1.52	-7.49	17.58	
	15	CZ01	6.67	0.47	120.00	0.84	35.15	20.99	13.39	117.50	11.88	23.66	-3.78	-20.84	9.38	-1.18	-2.20	-1.81	-8.17	27.75	
	19	GCO1	7.30	0.76	415.00	0.93	80.78	8.42	47.60	25.96	5.02	5.36	45.87	-3.73	-19.04	10.82	0.32	0.74	-2.92	-8.93	22.47
	20	ABA01	7.36	0.51	280.00	2.08	50.72	4.97	25.96	2.22	3.44	28.93	4.66	-3.98	-21.91	9.97	0.05	0.21	-3.38	-9.34	13.20
	21	CS01	6.44	0.19	85.00	2.52	9.06	16.14	23.96	10.80	15.16	15.16	4.66	-3.96	-20.60	11.07	-2.04	-4.02	-3.24	-8.15	33.39
	22	DP02	8.63	0.31	110.00	8.17	17.09	47.71	35.87	4.03	7.88	18.22	8.70	-0.12	-3.44	-2.51	0.46	0.98	-3.46	-7.61	0.27
	24	DF01	5.90	0.12	40.00	2.53	3.37	7.88	20.68	1.28	9.78	3.70	3.70	-4.02	-21.26	10.94	-3.30	-6.21	-4.53	-8.64	54.50
	26	ROD02	6.06	0.08	45.00	0.41	2.30	1.70	2.96	1.35	2.63	4.89	4.89	-4.72	-25.61	12.16	-3.24	-5.81	-4.66	-9.87	42.41
	27	EF02	6.70	0.11	65.00	0.65	5.92	1.39	1.28	1.72	5.83	5.10	5.10	-1.30	-9.98	0.39	-2.05	-3.82	-4.17	-9.62	14.03
	28	BB01	7.05	0.04	55.00	0.65	2.26	1.11	1.06	0.77	1.99	0.98	0.98	-1.77	-10.57	3.58	-2.17	-4.35	-4.88	-10.18	5.30
	29	VK02	5.76	0.06	12.50	0.35	3.85	0.47	1.63	0.97	0.97	0.91	2.47	-4.27	-23.76	10.43	-3.85	-7.55	-4.54	-10.89	23.51
	30	BB02	6.22	0.19	50.00	1.66	10.44	14.99	26.28	2.23	5.34	8.79	8.79	-4.51	-24.16	11.91	-2.42	-4.56	-3.86	-8.64	32.60
	31	VK04	6.45	0.07	42.50	0.38	5.86	0.66	0.28	1.02	1.01	2.68	2.68	-4.66	-25.73	11.52	-2.47	-4.93	-4.37	-10.70	16.32
	32	GR01	5.85	0.05	22.50	0.34	0.80	2.31	8.71	0.38	1.65	1.34	1.34	-4.27	-20.01	14.13	-4.19	-7.80	-5.62	-9.93	34.39
	33	TA02	6.25	0.06	22.50	0.65	3.23	0.61	2.12	2.12	0.59	1.07	2.64	-4.32	-24.33	10.27	-3.19	-6.12	-4.84	-10.70	13.69
	34	GR03	6.29	0.04	20.00	0.39	1.42	0.94	2.21	5.52	1.36	1.32	10.48	-4.98	-27.18	12.68	-3.55	-6.72	-4.86	-10.16	11.10
	35	PV01	6.79	0.19	107.50	0.33	14.46	1.24	5.52	22.03	219.59	46.12	31.91	-4.60	-25.46	11.34	-1.39	-2.56	-3.95	-10.33	18.86
	36	GP01	7.08	0.82	190.00	3.70	71.35	39.37	22.03	0.28	0.38	0.91	0.98	-2.74	-13.73	8.18	-0.34	-0.69	-1.35	-7.33	17.08
			Min	5.76	0.04	12.50	0.33	0.80	0.47	0.28	0.38	0.91	0.98	-4.98	-27.18	-2.51	-4.19	-7.80	-5.62	-10.89	0.27
			Max	8.63	0.82	415.00	8.17	80.78	47.71	63.44	219.59	46.12	45.87	-0.12	-3.44	14.13	0.46	0.98	-1.35	-7.33	54.50
			Mean	6.63	0.27	105.66	1.62	21.10	11.84	16.52	28.17	9.03	12.68	-3.62	-19.81	9.15	-1.95	-3.69	-3.75	-9.22	23.83
			SD	0.70	0.27	108.67	1.88	26.63	15.35	17.69	62.84	11.59	14.32	1.30	6.37	4.25	1.47	2.83	1.20	1.15	15.00
			CV%	10.54	100.91	102.85	115.57	126.21	129.69	107.05	223.08	128.34	112.89	-35.82	-32.14	46.48	-75.55	-76.82	-31.99	-12.48	62.94

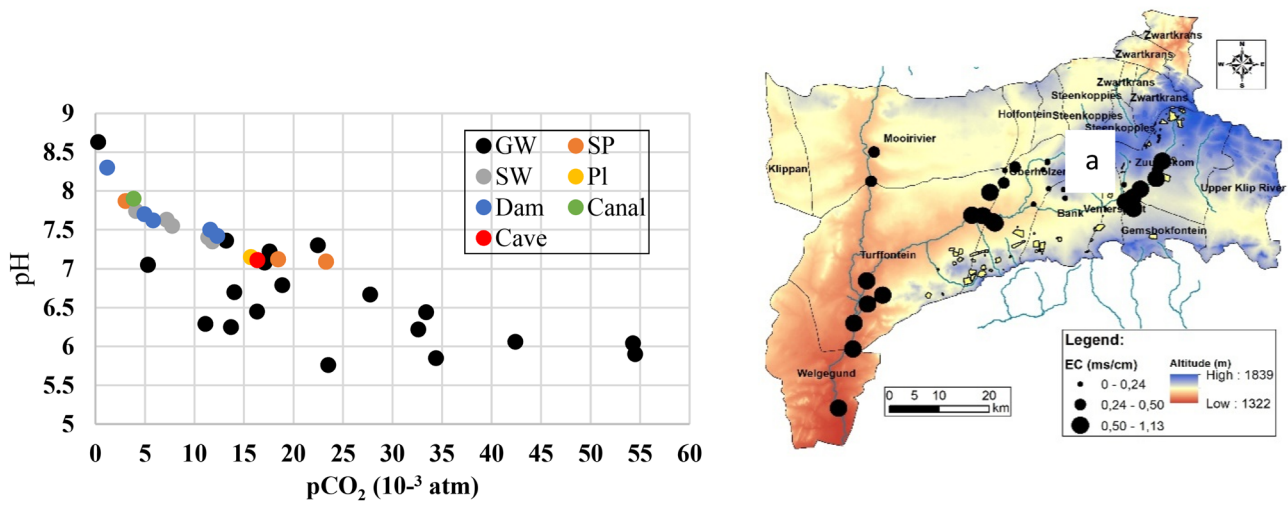
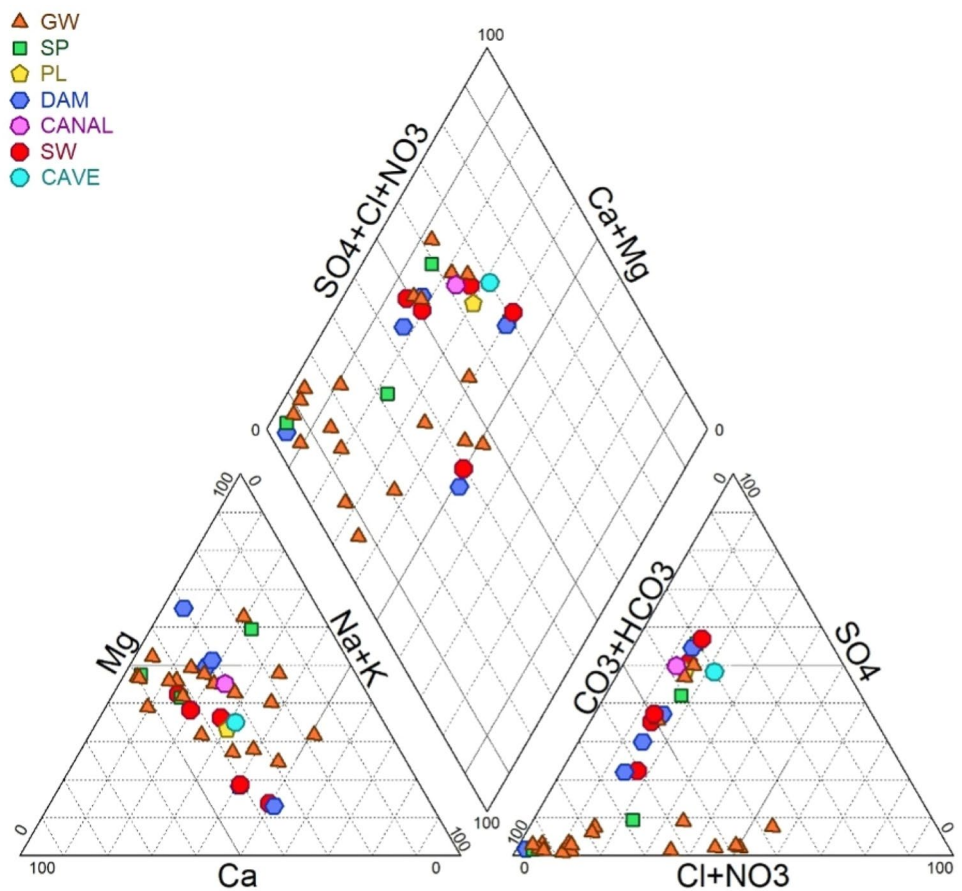


Fig. 5 a Plot of $p\text{CO}_2$ versus pH in study area, b spatial distributions of EC in study area

Fig. 6 Piper diagram of the region

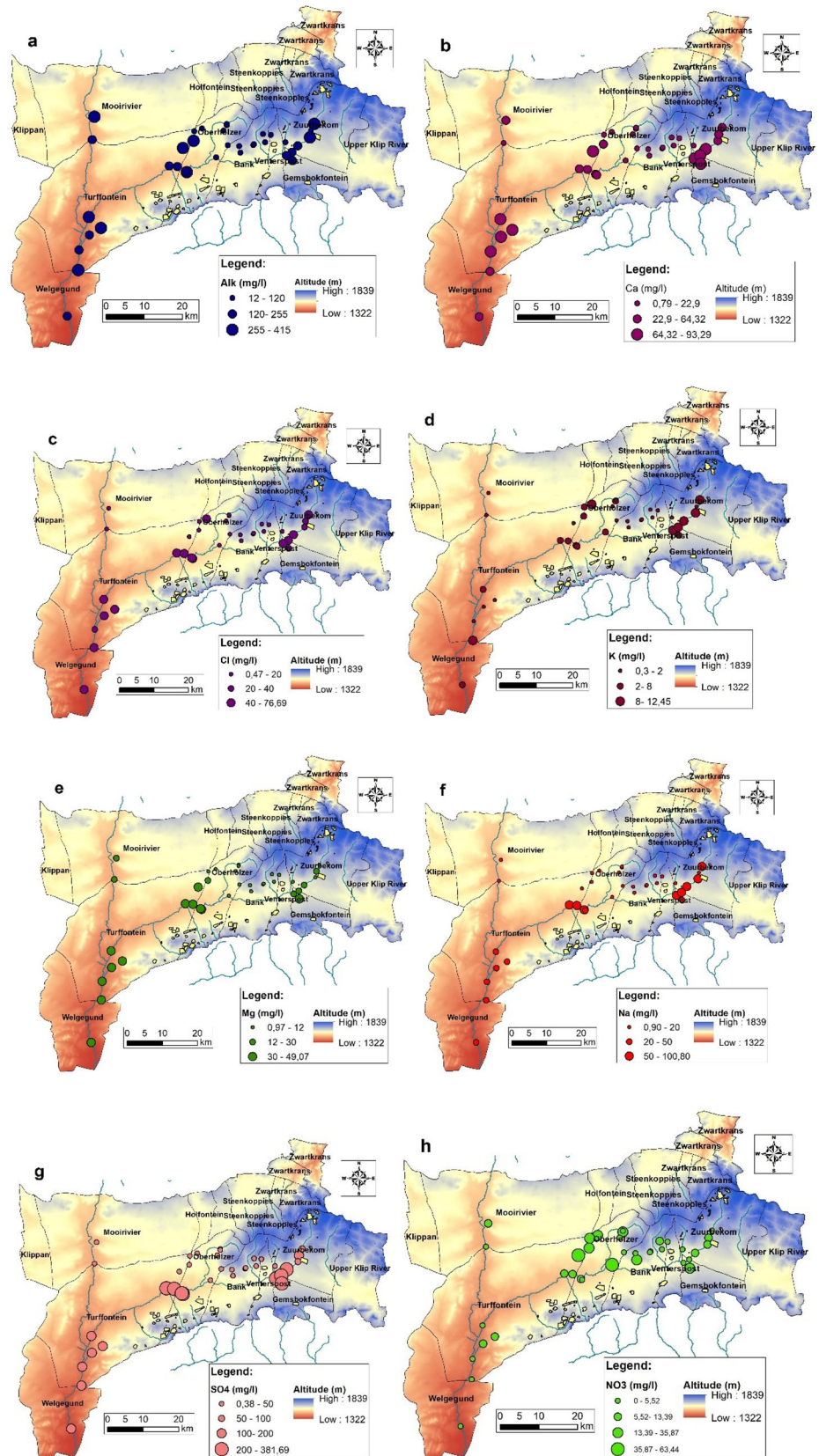


Major ions distributions

The distribution maps of the major (anion and cation) ions in study area were generated using Geographic Information

System (GIS) with Arc GIS 10.6.1 software. The spatial variation of Alkalinity and Ca^+ concentrations (Fig. 7a, b) indicates that the highest contents were located near WFS. However, these high concentrations were found in surface

Fig. 7 Spatial distributions of the major ions



water, springs and dams. Therefore, the contents of alkalinity and Ca^+ reach the discharge zones of study area. Chloride concentrations for all types of water ranged from 0.47–76.69 mg/l. The highest contents (40–76.69 mg/l) were registered in the surface water samples and near dykes. The high chloride concentrations may be due to short flow paths caused by the dykes in the study area (Fig. 7c). The high concentrations of potassium were observed in the water samples located at the Upper Wonderfonteinspruit Sub Regions (8–12 mg/l) and Boskop Dam (9.59 mg/l) downstream of the study area (Fig. 7d). The highest contents of K^+ are probably induced by weathering of K-feldspar minerals. The Mg ions in water samples ranged from 0.9 to 49 mg/l (Fig. 7e). The highest concentration was found in the lower WFS (30–49.07 mg/l). The ion exchange, weathering of ferromagnesium minerals, alteration and dissolution of dolomite of Malmani formation and precipitation of CaCO_3 could be the reasons behind the high magnesium concentration. Spatial variation of Na^+ (Fig. 7f) signifies that the highest concentration was registered upstream and in the centre of the WFS. Besides alteration and dissolution of halite minerals, agricultural and industrial activities might be the reason for high sodium contents in the region. The values of sulphate in water samples varied from 0.38 to 381.7 mg/l with an average of 96 mg/l (Fig. 7g). The highest concentrations of SO_4 were observed upstream of the study area close to Westonaria and in canal, cave and pipeline samples. The elevated SO_4 contents (200–381.7 mg/l) may be attributed to dissolution of gypsum and anhydrite minerals. Higher sulphates also suggest a human influence

due to industrial discharge (anthropogenic contamination). Acid mine drainage in the study area is associated with gold mining activities. It originates from sulphides such as pyrite found in many deposited ore bodies, which are oxidized after being exposed to atmospheric oxygen in the mining process (Barnard 2000). The water pollution by nitrate is a matter of high concern as it can negatively impact ecosystems and water supply. NO_3^- ion is a familiar pollutant in water (Darwish et al. 2011; Hamed and Dhahri 2013; Mokadem et al. 2015, 2016; Das et al. 2017). In the study area (Fig. 7h), the concentration of nitrate ranges from 0.1 to 63.4 mg/l with a mean of 25.66 mg/l. The highest contents were observed in the majority of groundwater samples (35–63.4 mg/l) which coincides with agricultural areas. The found concentrations exceed the acceptable limit of WHO 2006. The main factors that determine the high concentration of NO_3^- are anthropogenic activities such as agricultural practices, growing water demand, industrial waste deposits and return flow irrigation (Wang 2006; Mokadem et al. 2016).

Hydrochemical processes

Several hydrochemical analysis techniques, such as bivariate plots, were used to illustrate the hydrochemical processes controlling water chemistry in WFS valley. The passage of ions from rock to water takes place by leaching and dissolution. Figure 8a illustrates the relationship between Cl^- versus Na^+ ions, showing a correlation coefficient ($R^2=0.7$) that indicates halite dissolution, especially in groundwater samples. Most of the water samples in the area fall below

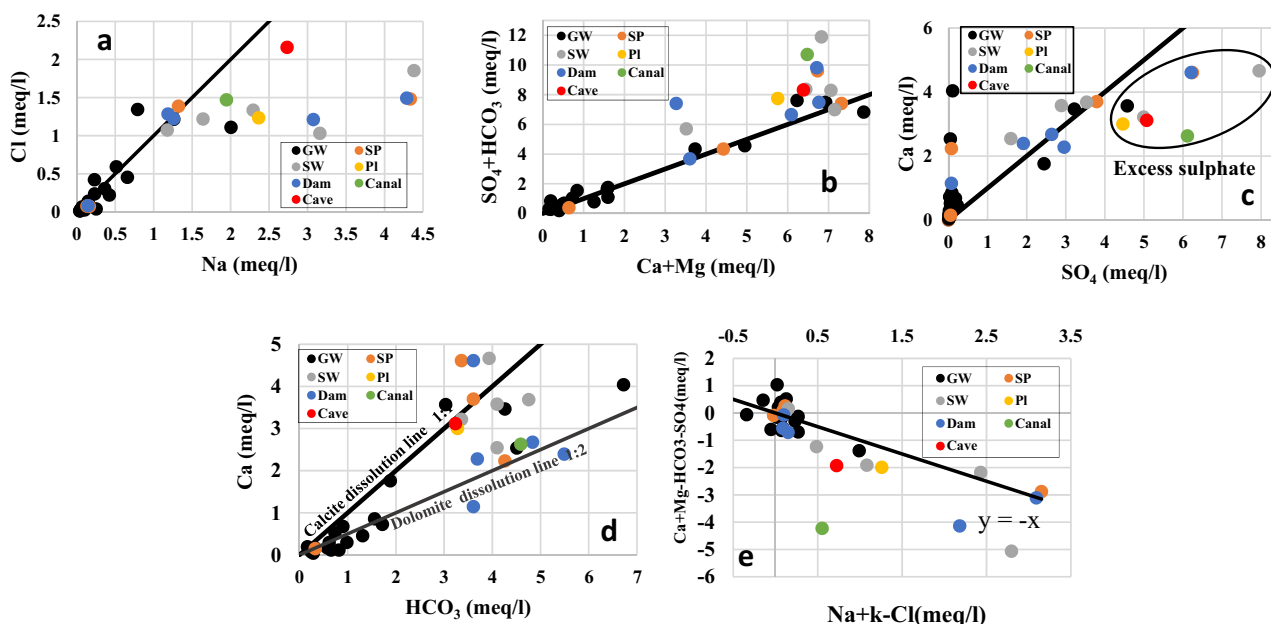
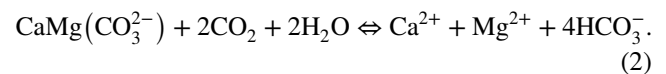
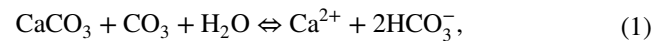


Fig. 8 Relationships between the major ions concentration ratios of water in the area

the 1:1 line revealing that water types are characterized by an excess concentration of Na^+ over Cl^- . This excess of sodium is sourced from the mechanism of rock weathering (silicate weathering: plagioclase or orthoclase) and ion exchange reactions (Meybeck 1987) which operate via the clay residual material of faults filling and metamorphic rocks in the study area, that fixes the sodium ions and releases the calcium ions. According to Chea et al. (2007) the high HCO_3^- alkaline conditions in the water allow the precipitation of Mg and Ca in the form of dolomite and calcite easier. The plot of $(\text{Ca}^{2+} + \text{Mg}^{2+})$ versus $(\text{HCO}_3^- + \text{SO}_4^{2-})$ diagram (Fig. 8b) gives an insight regarding the contribution of principal minerals and the influence of dissolution of carbonates (calcite, dolomite) and evaporates (gypsum) in the water of study area (Kumar et al. 2006; Mokadem et al. 2015, 2016). The majority of water points, especially for groundwater samples, plot along the equiline (1:1) suggesting the dissolution of dolomite and calcite and some samples that plot far from equiline (1:1) maybe due to other sources such as the activities of mining. The $\text{Ca}^{2+}/\text{SO}_4^{2-}$ ratio (Fig. 8c) illustrates approximately 60% of water in the samples around the 1:1 line, and reveals that these samples were influenced by gypsum dissolution. However, the rest of the water samples plot below the 1:1 line may possibly be caused by reserve ion exchange and industrial activities. These point samples have an excess of sulphate ions due

to sulphuric acid mine drainage (AMD) reacting with the alkaline dolomite and limestone of Malmani aquifer in the region. The plot of Ca^{2+} vs. HCO_3^- (Fig. 8d), shows two lines (1:1 and 1:2) the line 1:1 indicates the influence of calcite dissolution and the line 1:2 suggests the influence of dolomite dissolution. The water samples with the Ca^{2+} to HCO_3^- ratio which are controlled by calcite–dolomite dissolution and that most of the groundwater samples (Malmani aquifer) indicate the dolomite dissolution, according to the following reactions:



The relationship between $(\text{Na} + \text{K} - \text{Cl})$ and $(\text{Ca} + \text{Mg} - \text{HCO}_3 - \text{SO}_4)$ is used to explain this ion exchange (McLean et al. 2000; Mokadem et al. 2014, 2016). This plot shows that the majority of water points are close to the straight line of slope -1 (Fig. 8e), indicating the presence of an exchange between Na^+ , Mg^{2+} and Ca^{2+} in the water of the area. Figure 9a, b presents the Na-normalized bivariate plots of $\text{Mg}^{2+}/\text{Na}^+$ vs. $\text{Ca}^{2+}/\text{Na}^+$ and $\text{HCO}_3^-/\text{Na}^+$ vs. $\text{Ca}^{2+}/\text{Na}^+$ (Gaillardet et al. 1999a, b; Hagedorn and Whittier 2015). Most of the water points in the study area are influenced

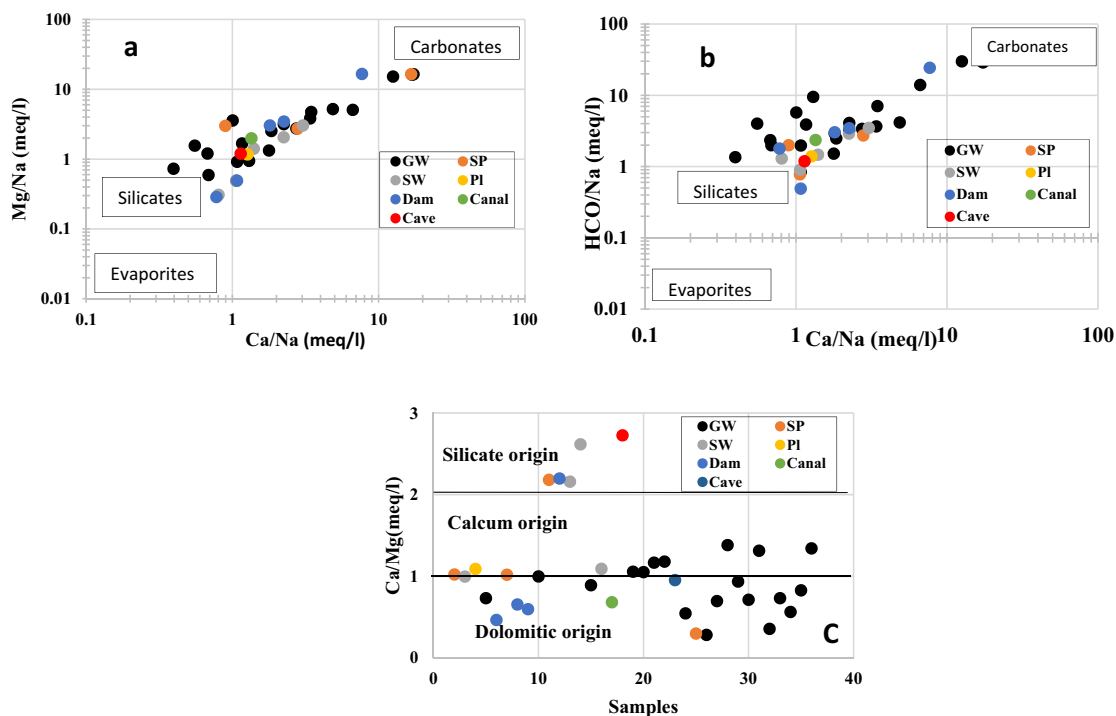


Fig. 9 a, b Water dissolved load diagrams c plot of samples versus (Ca/Mg) in study area

by carbonate dissolution and few samples indicate a silicate weathering process. However, comparing the obtained results, it must be noted that there is a predominance of carbonate dissolution (dolomite and calcite) over silicate weathering that is mainly associated with cations (Ca and Mg) dissolution. These cations (Ca and Mg) mainly originate from dolomite of Malmani formation in the region. The deficit in calcium and magnesium over sulphate and bicarbonate and the excess of sodium than chloride can be explained by ion exchange. 50% of water points (Fig. 9c) illustrate Ca/Mg ratio between 0 and 1 indicating dolomite dissolution, 37% of water samples fall between 1 and 2 suggesting calcite dissolution and 13% of water samples (5 samples) indicate a silicate origin.

The plot of nitrate versus chloride (Fig. 10) was established to evaluate the nitrate sources qualitatively (anthropogenic activities like agricultural and industrial) in the study area. The water samples on the NO₃⁻/Cl⁻ diagram fall mostly within case 1, characterized by having low NO₃⁻ and low Cl⁻ concentrations, indicating the absence of the influence of human activities. Half the groundwater samples belong in case 2, with high NO₃⁻ and low Cl⁻ concentrations, suggesting there are agricultural activities, unlike the situation with no water points observed in cases 3 and 4.

Saturation index (SI)

In the WFS valley, the saturation indexes are important to the equilibrium (or saturation state) and reactivity between minerals and groundwater from the water points data (Sandow et al. 2011). According to Garrels and Mackenzie (1967), the saturation indices of the minerals phase are obtained using the following equation:

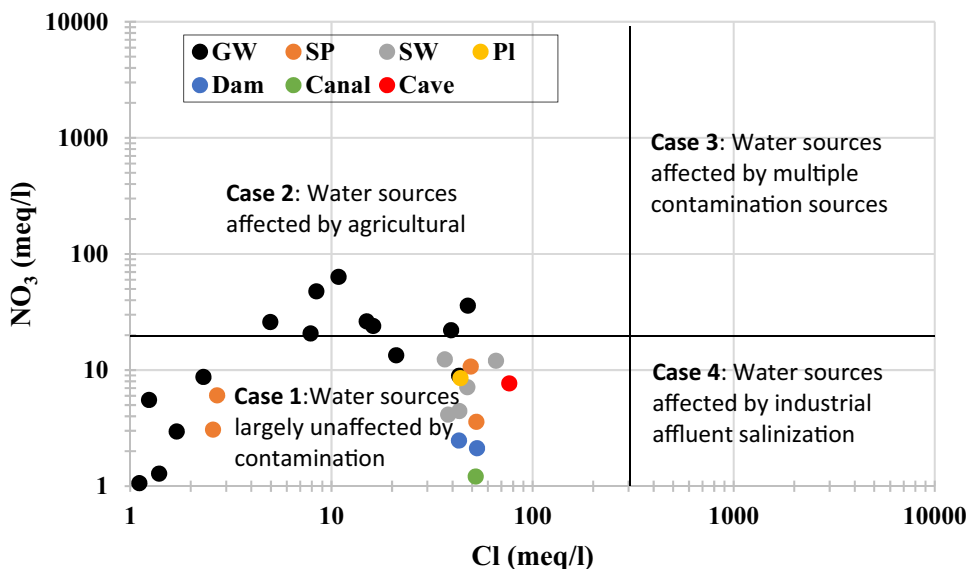
$$SI = \log (IAP/K),$$

where SI Saturation Index, IAP Ion Activity Product, *K* Equilibrium constant.

When SI value is 0, the mineral then is a saturation state (equilibrium state) with water, a calculated SI value > 0 suggests oversaturation compared to the particular mineral phase and can precipitate to reach equilibrium. A SI value < 0 indicates under saturation and that dissolution of the mineral will occur (Truesdell and Jones 1973; Zhang et al. 2016a, b).

Figure 11a and Table 1 present the saturation indices for minerals phases (Halite (NaCl), Calcite (CaCO₃), Dolomite (CaMg (CO₃)₂), Gypsum (NaCl)) from water types in the WFS valley. Figure 10a shows that all water points are under saturated with respect to gypsum and halite and half of the samples are saturated to oversaturated with respect to calcite and dolomite. These oversaturated samples include springs, dams and surface waters of the area. Calcite and dolomite in Fig. 10a illustrated the same curve. The relationship between saturation indices (SI) of calcite, dolomite, gypsum and halite and their ions are shown in Fig. 11b–e. Figure 11b, c illustrates a good correlation of gypsum and halite, indicating the possible dissolution of these minerals and that the water for the study area has not attained equilibrium with the mineral phases. The positive value of springs, dams, surface waters and canal of saturation indices for dolomite and calcite mineral phases (Fig. 11d, e) indicates that they are oversaturated. An oversaturation can influence the water chemistry and lead to precipitation of Ca²⁺ and Ca²⁺–Mg²⁺, which explains the presence of dolomite (Malmani group) and limestone in the lithology of the study area. On the other hand, the groundwaters were under saturation with respect

Fig. 10 Plot of NO₃ versus Cl in study area



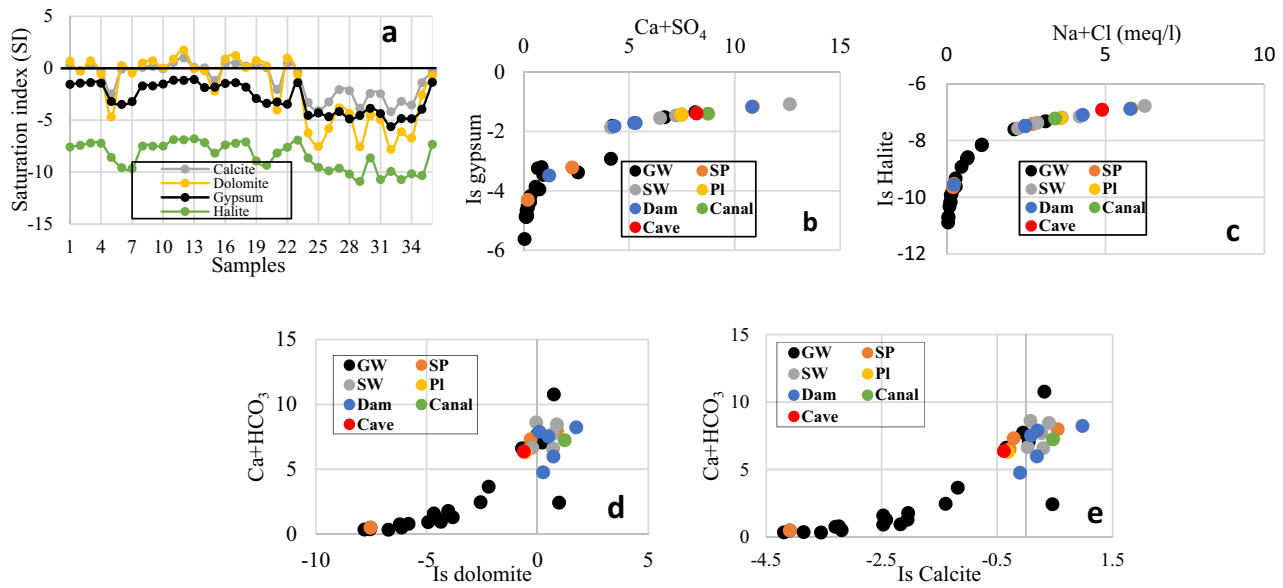


Fig. 11 Plot of the saturation indexes in study

Table 2 Isotope of precipitation

Months	Nov		Jan		Feb		March		April		June	
	$\delta^{18}\text{O}$	$\delta^2\text{H}$	$\delta^{18}\text{O}$	$\delta^2\text{H}$	$\delta^{18}\text{O}$	$\delta^2\text{H}$	$\delta^{18}\text{O}$	$\delta^2\text{H}$	$\delta^{18}\text{O}$	$\delta^2\text{H}$	$\delta^{18}\text{O}$	$\delta^2\text{H}$
1	-1.17	-3.34	-4.49	-27.33	0.12	10.54	-1.29	-9.16	-1.88	-8.72	-3.72	-11.00
2	-0.53	1.39	-2.58	-21.13	0.16	12.57	-2.96	-12.16	-3.82	-19.78	-3.71	-10.35
3	-2.99	-10.51	-4.06	-23.41	0.38	13.31	-1.53	-5.02	-2.95	-15.96	-0.91	1.96
4	-1.10	-0.06	-3.87	-24.00	-0.08	14.96	-3.51	-15.81	-1.57	-9.89		

to calcite and dolomite, suggesting the dissolution of these minerals, shorter flow path and residence time in the aquifer.

Stable isotope results

Precipitation

Precipitation samples in the WFS valley ($n=46$) were collected during six periods (November 2018, January 2019, February 2019, March 2019, April 2019, June 2019) from four locations S1, S2, S3 and S4 with different altitudes 1540, 1508, 1600 and 1353 m, respectively (Fig. 1c, Table 2). The isotopic composition of precipitation in this region ranged between -4.49 to 0.38‰ with mean -1.48‰ for $\delta^{18}\text{O}$ and -27.33 to 14.96‰ with mean -6.20‰ for $\delta^2\text{H}$. The regression equation of the Local Meteoric Water Line (LMWL) is: $\delta^2\text{H} = 7.39 * \delta^{18}\text{O} + 7.92\text{‰}$ ($R^2 = 0.85$) (Fig. 12). The slope and intercept of the LMWL are lower than those of the global meteoric water line (GMWL): $\delta^2\text{H} = 8\delta^{18}\text{O} + 10$ (Craig 1961), indicating the modification due to evaporation.

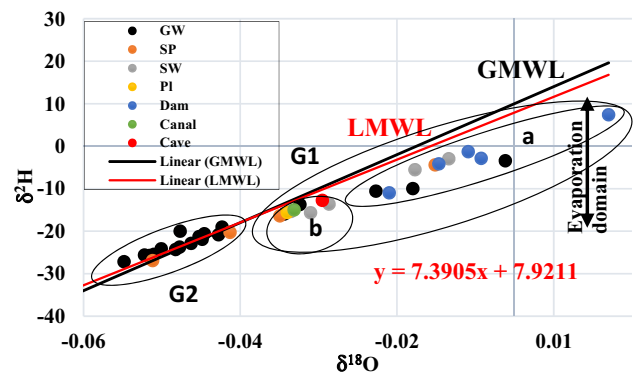


Fig. 12 Plot of $\delta^{18}\text{O}$ vs $\delta^2\text{H}$ in the study area

Water samples

The surface waters ($n=4$) show an isotopic composition varying from -2.85 to -0.83‰ and -15.66 to -2.97‰ for $\delta^{18}\text{O}$ and $\delta^2\text{H}$, respectively. Dam waters ($n=5$) have $\delta^{18}\text{O}$, ranging between -1.59 and 1.2‰ and $\delta^2\text{H}$ ranging between

−10.98 and 7.3‰. Spring samples ($n=5$) of the region, isotopic composition varied from ($\delta^{18}\text{O}=-4.61$ to $-10.1‰$ and $\delta^2\text{H}=-26.9$ to $-4.39‰$). Groundwater points ($n=19$) show $\delta^2\text{H}$ composition varying from -27.18 to $-3.44‰$ of the mean $-19.81‰$ and for $\delta^{18}\text{O}$ from -4.98 to $-0.11‰$ of the mean $-3.62‰$. Canal, pipeline and cave samples have $\delta^{18}\text{O}$ ($-2.81‰$, $-2.9‰$ and $-2.45‰$) and $\delta^2\text{H}$ ($-15.01‰$, $-15.58‰$ and $-12.75‰$) respectively. The isotopic composition of waters measured in the study area is shown in the conventional $\delta^2\text{H}‰$ vs $\delta^{18}\text{O}‰$ plot (Fig. 12). All the water samples in this region were below and near the LMWL which indicates they were from local precipitation and recent water from the dolomitic system. Based on distribution of the positions of the data points on $\delta^2\text{H}$ and $\delta^{18}\text{O}$ diagram (Fig. 12) are two groups may be clearly distinguished.

- The first group (1) is situated under the GMWL. This group comprises two subgroups: group (a) and group (b). The group (a) encloses the samples (all of the Dams, Gemsbokfontein Spring, 2 surface waters and 3 groundwaters (22,27,28) which are mostly located upstream, except for the two dams (Potchefstroom and Boskop dams) which are located downstream of the study area (Fig. 1c).
- The group (b) named also mixing water includes (Gerhard Minnebron spring, 2 groundwaters (10,36), 2 surface waters, 1 canal, 1 Pipeline and 1 cave. Therefore, the group (a) is richer in isotopes than group (b). The slope and the regression line interception of first group samples are below the GMWL and LMWL (Evaporation line $\delta\text{D}=5.48 \delta^{18}\text{O}+0.0005‰$). This means that water samples undergo evaporation (Tsujimura et al. 2007).
- Group b mixes water between the water of the area and rainwater. This mixture of water is associated to the percolation via the fault such as the cave and spring samples, irrigation processes (groundwater samples) and a mixing mechanism from the surface water and also from pipeline canals after dewatering.

- The second group (2) is represented mainly by the remaining wells. This group contains the majority of groundwaters samples, Bovenste and ROD01 springs. These values of $\delta^2\text{H}$ and $\delta^{18}\text{O}$ are relatively low compared to those of the first group. The values of this group indicate that groundwater recharge is influenced by the rainfall with rapid infiltration and by river flow such as WFS, Middelvlleispruit and Renfonteinspruit.

According to Dansgaard (1964), the intercept of the GMWL is named the deuterium excess, and was defined as $d\text{-excess} (‰)=\delta^2\text{H}-8*\delta^{18}\text{O}$. This last one is acquired during evaporation and does not vary significantly during the later history of the atmospheric moisture. It is a useful indicator for identifying secondary processes influencing the atmospheric vapor content in the evaporation–condensation cycle (Craig 1961; Machavaram and Krishnamurthy 1995; Celle-Jeanton et al.2001). These d-excess values in the study area ranging between -2.22 to $12.68‰$ suggest that the isotopic composition in water points are characteristic of a semi-arid climate. The d-excess value is also an index indicating the evaporation effect on the physicochemical characteristics of water: if the d-excess decreases, the water evaporates, (Craig 1961; Merlivat and Jouzel 1979; Gat and Matsui 1991; Machavaram and Krishnamurthy 1995; Tsujimura et al. 2007; Mokadem et al. 2016; Dassi et al. 2018). The relationship between d-excess and $\delta^{18}\text{O}$ shown in Fig. 13a. This diagram illustrated two groups (G1, G2), Group1 showing d-excess -2.51 to $8.17‰$ and $\delta^{18}\text{O} < -2.73‰$ to $-0.11‰$. So between lower d-excess and enriched $\delta^{18}\text{O}$ indicated there are significant modifications due to kinetic evaporation of the precipitated water before groundwater recharge, and this also signifies that groundwater samples are fed principally by the return flow of irrigation water. Group 2 shows an isotopic signature d-excess 8.75 to $14.13‰$ and $\delta^{18}\text{O} -4.26$ to $-3.63‰$, this group indicates rapid infiltration of meteoric water into the Malmani aquifer. Cl vs $\delta^{18}\text{O}$ scatter plot (Fig. 13b) is another way to identify the water processes as

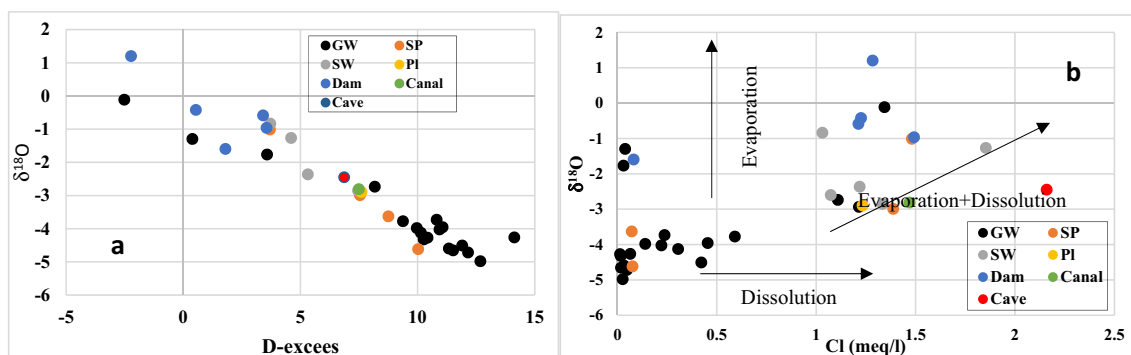


Fig. 13 a Plot of $\delta^{18}\text{O}$ vs D-excess, b plot of $\delta^{18}\text{O}$ vs Cl in the study area

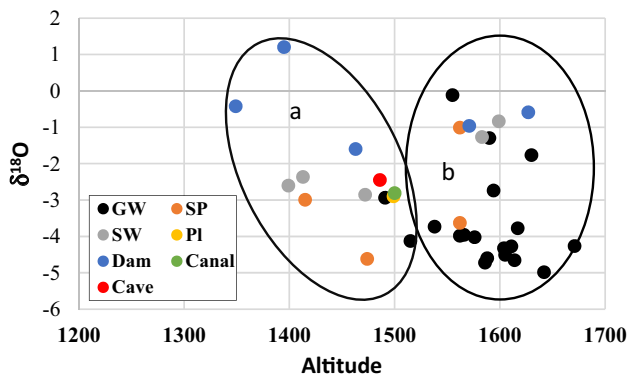


Fig. 14 $\delta^{18}\text{O}$ plotted versus altitude in study area

rock-water interactions. Many recharge sources with various ^{18}O values might be suggested. These sources are influenced by the hydraulic continuity between the different Compartments, leaching during runoff and/or leakage from Malmani aquifer through the Karst system which facilitates the water movement and flow. Figure 13b presents two groups. Group one points out an evaporation signature and high concentrations of chloride. This high concentration indicates that the chloride obtained by anthropogenic contamination such as industrial discharge (high concentration of sulphate). Group two samples included the groundwater points from Malmani aquifer show a good correlation and indicate the dissolution of evaporative (halite, anhydrite and gypsum) with a low concentration of chloride.

Figure 14 illustrates the results $\delta^{18}\text{O}$ versus altitude. This result shows two groups (a, b). Group (a) suggests the diffuse recharge at low altitude (< 1500 m) within downstream of the study area. Group (b) encloses (the majority of groundwater samples, Gemsbokfontein and Bovenste Springs and Donaldson and Luipaardsvlei Dams) at high altitude which is mostly located upstream of the region suggest high altitude recharging water. The altitude effect is calculated by the relation between mean precipitation isotope values for the four stations and elevation in meters (h) highlighting a depletion of heavy stable isotopes of about -0.16‰ per 100 m elevation for $\delta^{18}\text{O}$, indicating the rapid groundwater recharge through the karstic system for all the water points regardless of their source. Therefore, the WFS catchment is principally fed by rainwater.

Conclusion

This research was conducted to understand the hydrochemical and isotopic relations in the WFS. According to the piper diagram, two main hydrochemical facies are in the study area: (1) Ca-Mg-Cl-SO_4 ; (2) Ca-Mg-HCO_3 . Water points generally have lower EC and pH and high concentrations

of ions HCO_3 , SO_4 and Ca in surface water, springs, dams, canals and pipelines. The results of major ions (HCO_3 , SO_4 , Ca, Cl, Mg, Na, NO_3) after using various bivariate plots such as (Cl^- vs Na^+ , ($\text{Ca}^{2+} + \text{Mg}^{2+}$) vs ($\text{HCO}_3^- + \text{SO}_4^{2-}$), Ca^{2+} vs SO_4^{2-} , NO_3^- vs Cl) showing in this area that mineral dissolution, ion exchange, weathering, evaporation, agriculture nitrification and mining activities are the principal controlling processes. The results of the saturation index present an appropriate hydrogeochemical environment for evaporate (halite and gypsum) dissolution (less than zero) and carbonate (calcite and dolomite) dissolution/precipitation. The LMWL carried out with measurement during six periods was $\delta^2\text{H} = 7.39 * \delta^{18}\text{O} + 7.9\text{‰}$ ($R^2 = 0.85$) which is close to the GMWL. The $\delta^2\text{H}$ and $\delta^{18}\text{O}$ values of water samples confirm that the water of the karst system (Malmani aquifer) is of meteoric origin and recent water and the majority of groundwater are derived from the rapid infiltration of local precipitation.

Acknowledgements The authors would like to thank Christian Steyn, Neil Kriel and Theuns van Wyk for their assistance with samples collection

References

- Abyie TA, Mengistu H, Demlie MB (2011) Groundwater resource in the crystalline rocks of the Johannesburg area, South Africa. *J Water Resour Prot* 3:199–211
- Al-Khashman OA (2008) Assessment of the spring water quality in The Shoubak area, Jordan. *Environmentalist* 28:203–215
- Allan JA (2002) *The Middle East Water question: hydropolitics and the global economy*. I.B. Tauris Publishers, London, New York
- Ayadi Y, Mokadem N, Besser H, Khelifi F, Harabi S, Hamad A, Boyce A, Laouar R, Hamed Y (2018a) Hydrochemistry and stable isotopes ($\delta^{18}\text{O}$ and $\delta^2\text{H}$) tools applied to the study of karst aquifers in southern Mediterranean basin (Teboursouk area, NW Tunisia). *J Afr Earth Sci* 137:208–217. <https://doi.org/10.1016/j.jafrearsci.2017.10.018>
- Ayadi Y, Mokadem N, Besser H, Redhaounia B, Khelifi F, Harabi S, Nasri T, Hamed Y (2018b) Statistical and geochemical assessment of groundwater quality in Teboursouk area (Northwestern Tunisia Atlas). *J Environ Earth Sci* 77:349. <https://doi.org/10.1007/s12665-018-7523-2>
- Barbecot F, Marlin C, Gibert E, Dever L (2000) Hydrochemical and isotopic characterization of the Bathonian and Bajocian coastal aquifer of the Caen area (northern France). *Appl Geochem* 15:791–805
- Barnard HC (2000) *An Explanation of the 1:500 000 General Hydrogeological Map*. Johannesburg 2526. Department of Water Affairs and Forestry
- Belkhir L, Boudoukha A, Mouni L (2010) Application of multivariate statistical methods for characterization of groundwater—a case study: Ain Azel Plain (Algeria). *Geoderma* 159:390–398
- Bredenkamp DB (1993) Hydrological Evaluation of the West Rand dolomitic compartments: Zuurbekom, Gemsbokfontein East and Gemsbokfontein West. DWAf, Pretoria
- Brink ABA (1979) *Engineering geology of South Africa*, vol 1. Building Publications, Pretoria, p 319

- Buttrick DB, Van Schalkwyk A, Kleywegt RJ, Watermeyer RB (2001) Proposed method for dolomite land hazard and risk assessment in South Africa. *J South African Inst Civil Eng* 43(2):27–36
- Celle-Jeanton H, Travi Y, Blavoux B (2001) Isotopic typology of the precipitation in the Western Mediterranean region at the three different time scales. *Geophys Res Lett* 28:1215–1218. <https://doi.org/10.1029/2000GL012407>
- Chea GT, Yun ST, Mayer B, Kim KH, Kim SY, Kwon JS, Kim K, Koh YK (2007) Fluorine geochemistry in bedrock groundwater of South Korea. *Sci Total Environ* 385(1–3):272–283
- Clark I, Fritz P (1997) *Environmental isotopes in hydrogeology*. Lewis Publishers, New York, p 328
- Coetzee H, Wade PW, Ntsume G, Jordaan W (2002) Radioactivity study on sediments in a dam in the Wonderfontein spruit catchment. DWAF-Report 2002, Pretoria, South Africa
- Coetzee H, Wade P, Winde F (2006a) An assessment of sources, pathways, mechanisms and risks of current and future pollution of water and sediments in the Wonderfontein spruit Catchment. WRC Report No 1214/1/06, ISBN No 1-77005-419-7
- Coetzee H, Winde F, Wade PW (2006b) An assessment of sources, pathways, mechanisms and risks of current and potential future pollution of water and sediments in gold-mining areas of the Wonderfontein spruit Catchment. WRC, Pretoria
- Cole DI (1998) Uranium. In: Wilson MGC, Anhaeusser CR (eds) *Mineral resources of South Africa*. Council for Geoscience Handbook, vol 16, pp 642–658
- Connor JA, Paquette S, Mchugh T, Gie E, Hemingway M, Bianchi G (2017) Application of natural resource valuation concepts for development of sustainable remediation plans for groundwater. *J Environ Manag* 204:721
- Craig H (1961) Isotopic variations in meteoric waters. *Science* 133(3465):1702–1703
- Dansgaard W (1964) Stable isotopes in precipitation. *Tellus* 4:436–468
- Darwish T, Atallah T, Francis R, Saab C, Jomaa I, Shaaban A, Sakka H, Zdruli P (2011) Observations on soil and groundwater contamination with nitrate: a case study from Lebanon-East Mediterranean. *Agric Water Manag* 99(1):74–84
- Das N, Sarma KP, Patel AK, Deka JP, Das A, Kumar A, Shea PJ, Kumar M (2017) Seasonal disparity in the co-occurrence of arsenic and fluoride in the aquifers of the Brahmaputra flood plains, Northeast India. *Environ Earth Sci* 76:183. <https://doi.org/10.1007/s12665-017-6488-x>
- Dassi L, Tarki M, El Mejri H, Ben Hammadi M (2018) Effect of over pumping and irrigation stress on hydrochemistry and hydrodynamics of a Saharan oasis groundwater system. *Hydrol Sci J* 63(2):227–250. <https://doi.org/10.1080/02626667.2017.1417595>
- De Klerk TC (2018) An integrated rainfall-runoff water quality model in a mine impacted karst environment. PhD thesis, Potchefstroom Campus of the North-West University, South Africa
- De Kock WP (1967) The dolomite eyes or fountains of the Wonderfontein Valley in western Transvaal. *Fauna Flora Pretoria* 18:56–66
- Dotsika E, Lykoudis S, Poutoukis D (2010) Spatial distribution of the isotopic composition of precipitation and spring water in Greece. *Glob Planet Chang* 71:141–149
- Dubois C, Quinif Y, Baele JM, Barriquand L, Bini A, Bruxelles L, Dandurand G, Havroni C, Kaufmann O, Lans B, Maire R, Martin J, Rodet J, Rowberry MD, Tognini P, Vergari A (2014) The process of ghost-rock karstification and its role in the formation of cave systems. *Earth Sci Rev* 131(2014):116–148
- Durand JF (2012) The impact of gold mining on the Witwatersrand on the rivers and karst system of Gauteng and North West Province, South Africa. *J Afr Earth Sc* 68:24–43
- Edet AE, Offiong OE (2002) Evaluation of water quality pollution indices for heavy metal contamination monitoring. A study case from Akpabuyo-Odukpani area, Lower Cross River Basin (southeastern Nigeria). *GeoJournal* 5:295–304
- Els BG (1987) The auriferous Middellevlei Reef depositional system, West Wits Line, Witwatersrand Supergroup. Rand Afrikaans University, Johannesburg
- Els BG (2000) Unconformities of the auriferous, Neoproterozoic Central Rand Group of South Africa: application to stratigraphy. *J Afr Earth Sci* 30:47–62
- Enslin JF, Kriel JP (1967) The assessment and possible future use of the dolomitic groundwater resources of the Far West Rand. Papers of the international conference on water and peace, vol 2. US Government Printing Office, Washington DC, pp 1–10
- Eriksson PG, Reczko BFF (1995) The sedimentary and tectonic setting of the Transvaal Supergroup floor rocks to the Bushveld complex. *J Afr Earth Sci* 21(4):487–504
- Faure G (1998) *Principles and applications of geochemistry*, 2nd edn. Prentice-Hall, Englewood Cliffs, NJ
- Fetter CW (2014) *Applied hydrogeology*, 4th edn. Pearson, UK
- Fleisher JNE (1981) The geohydrology of the dolomite aquifers of the Malmani Subgroup in the South-Western Transvaal, PhD thesis. Republic of South Africa. UFS, Bloemfontein
- Foster MBJ (1988) The groundwater resources of the Far West Rand dolomitic compartments. DWAF, Pretoria
- Gaillardet J, Dupre B, Allegre CJ (1999a) Geochemistry of large river suspended sediment: silicate weathering or recycling tracer? *Geochim Cosmochim Acta* 63(23–24):4037–4051
- Gaillardet J, Dupré B, Louvat P, Allegre CJ (1999b) Global silicate weathering and CO₂ consumption rates deduced from the chemistry of large rivers. *Chem Geol* 159(1–4):3–30
- Garrels RM, Mackenzie FT (1967) Origin of the chemical compositions of some springs and lakes. In: Stumm W (ed) *Equilibrium concepts in natural water systems*. American Chemical Society, Washington, pp 222–242
- Gat JR, Matsui E (1991) Atmospheric water balance in the Amazon Basin. An isotopic evapotranspiration model. *J Geophys Res* 96:1317913188. <https://doi.org/10.1029/91JD00054>
- Hagedorn B, Whittier RB (2015) Solute sources and water mixing in a flashy mountainous stream (Pahsimeroi River, U.S. Rocky Mountains): implications on chemical weathering rate and groundwater–surface water interaction. *Chem Geol* 391:123–137
- Hamed Y (2015) *Fonctionnement et dynamisme des ressources hydriques des aquifères en milieu aride à semi-aride: approche hydrogéologique, hydrochimique et isotopique*. HDR. Faculty of Sciences, Sfax, p 160
- Hamed Y, Dhahri F (2013) Hydro-geochemical and isotopic composition of groundwater and meteoric water, with emphasis on sources of salinity, in the aquifer system in Northwestern Tunisia. *J Afr Earth Sci*. <https://doi.org/10.1006/s22517-013-0313-3>
- Hodgson FDI, Usher BH, Scott R, Zeelie S, Cruywagen LM, De Necker E (2001) Prediction techniques and preventative measures relating to the post operational impact of underground mines on the quality and quantity of groundwater resources. Report no. 699/1/01. Water Research Commission, Pretoria
- IWQS (Institute for Water Quality Studies of the Department of Water Affairs and Forestry, South Africa) (1999) Report on the radioactivity monitoring programme in the Mooi River (Wonderfontein-spruit) catchment. Report no. N/C200/00/RPQ/2399. Department of Water Affairs and Forestry, Pretoria
- Jennings JE, Brink ABA, Louw A, Gowan GD (1965) Sinkholes and subsidences in the Transvaal dolomite of South Africa. In: Proc 6th international conference of soil mech. and found. eng., Montreal, pp 51–54
- Kumar M, Ramanathan AL, Rao MS, Kumar B (2006) Identification and evaluation of hydrogeochemical processes in the groundwater environment of Delhi, India. *Environ Geol* 50:1025–1039

- Ledesma-Ruiz R, Zapata EP, Parra R, Harter T, Mahlkencht J (2015) Investigation of the geochemical evolution of groundwater under agricultural land: a case study in northeastern Mexico. *J Hydrol* 521:410–423
- Machavaram MV, Krishnamurthy RV (1995) Earth surface-evaporative process: a case study from the Great Lakes region of the United States based on deuterium excess in precipitation. *J Geochim Cosmochim Acta* 59:4279–4283. [https://doi.org/10.1016/0016-7037\(95\)00256-Y](https://doi.org/10.1016/0016-7037(95)00256-Y)
- Mc Carthy T, Rubidge B (2005) *Earth and life*. Kumba Resources, Johannesburg
- Mclean W, Jankowski J, Lavit N (2000) Groundwater quality and sustainability in an alluvial aquifer, Australia. Groundwater, past achievement, and future challenges. A Balkema, Rotterdam, pp 567–573
- Merlivat L, Jouzel J (1979) Global climatic interpretation of the deuterium-oxygen 18 relationship for precipitation. *J Geophys Res* 84:50295033. <https://doi.org/10.1029/JC084iC08p05029>
- Meybeck M (1987) Global chemical weathering of surficial rocks estimated from river dissolved loads. *Am J Sci* 287(5):401–428
- Mokadem N, Hamed Y, Ben Saad A, Gargouri I (2014) Atmospheric pollution in North Africa (ecosystems–atmosphere interactions): a case study in the mining basin of El Guettar–M’Dilla (south-western Tunisia). *Arab J Geosci* 7:2071–2079
- Mokadem N, Hamed Y, Hfaïd M, Ben Dhia H (2015) Hydrogeochemical and isotope evidence of groundwater evolution in El Guettar Oasis area, Southwest Tunisia. *J Carbon Evap* 30:417–437. <https://doi.org/10.1007/s13146-015-0235-8>
- Mokadem N, Demdoum A, Hamed Y, Bouri S, Hadji R, Boyce A, Laouar R, Sâad S (2016) Hydrogeochemical and stable isotope data of groundwater of a multi-aquifer system: Northern Gafsa basin—Central Tunisia. *J Afr Earth Sci* 114:174–191. <https://doi.org/10.1016/j.jafrearsci.2015.11.010>
- Morsy KM, Morsy AM, Hassan AE (2018) Groundwater sustainability: opportunity out of threat. *Groundw Sustain Dev* 7:277–285
- Parkhurst DL, Appelo CAJ (1999) *User’s guide to PHREEQC (version 2)—a computer program for speciation, batch-reaction, one-dimensional transport, and inverse geochemical calculations*. US Geol. Surv. Water Resour. Invest. Rep. 99-4259
- Pazand K (2014) Geochemical and hydrogeochemical evolution of groundwater in Ferdows area, Northeast of Iran. *Environ Earth Sci* 71:685–695
- Pazand KJ, Sarvestani F (2013) Hydrogeochemical investigation in an arid region of Iran (Tabas, Central Iran). *Environ Earth Sci* 70:743–752
- Piper AM (1944) A graphic procedure in the geochemical interpretation of water analyses. *Trans Am Geophys Union* 25:914–923
- Robb LJ, Robb VM (1998) Gold in the Witwatersrand Basin. In: Wilsson MGC, Anhausser CR (eds) *The mineral resources of South Africa handbook*, vol 16. Council for Geoscience, Pretoria, pp 294–349
- Sandow MY, Banoeng-Yakubo B, Akabzaa T (2011) Characterization of the groundwater flow regime and hydrochemistry of groundwater from the Buem formation, eastern Ghana. *Hydrol Process* 25:2288–2301
- Schrader A and Winde F (2015) Unearthing a hidden treasure: 60 years of karst research in the Far West Rand, South Africa. *South Afr J Sci* 111 (5/6)
- Sharif MU, Davis RK, Steele KF, KimB KTM, Fazio JA (2008) Inverse geochemical modeling of groundwater evolution with emphasis on arsenic in the Mississippi River Valley alluvial aquifer, Arkansas (USA). *J Hydrol* 350:41–55
- Sissakian KV, Abdul Ahad AD, Al-Ansari N, Knutsso S (2016) Factors controlling the karstification process in the Fatha formation in Iraq. *J Earth Sci Geotech Eng* 6(3):147–162. ISSN: 1792-9040
- Swart CJU, James AR, Kleywegt RJ, Stoch EJ (2003a) The future of the dolomitic springs after mine closure on the Far West Rand, Gauteng. *RSA Environ Geol* 44:751–770. <https://doi.org/10.1007/s00254-003-0820-3>
- Swart CJU, Stoch E, Van Jaarsveld CF, Brink ABA (2003b) The lower Wonderfontein Spruit: an expose. *Environ Geol* 43:635–653
- Truesdell AH, Jones BF (1973) WATEQ, a computer program for calculating chemical equilibria of natural waters: NTIS PB2-20464, p 77
- Tsujimura M, Abe Y, Tanaka T, Shimada J, Higuchi S, Yamanaka T, Davaa G, Oyunbaatar D (2007) Stable isotopic and geochemical characteristics of groundwater in Kherlen River basin, a semiarid region in eastern Mongolia. *J Hydrol* 333:47–57
- Viljoen MJ, Reimold WU (2002) *An introduction to South Africa’s geological and mining heritage*. Geological Society and Mintek
- Wade PW, Woodborne S, Morris WM, Vos P, Jarvis NV (2002) Tier I risk assessment of selected radionuclides in sediments of the Mooi River catchment. WRC report no 1095/1/02. Water Research Commission, Pretoria
- Wang D (2006) Analysis on formation causes of nitrate contamination of shallow groundwater and control countermeasures in northern part of cretaceous ordos basin. *Groundwater* 26(4):12–15
- Wolmarans JF (1984) *Ontwikkeling van die dolomiet gebied aan die verre Wes-Rand: Gebeure in perspektief*, PhD thesis. UP, Pretoria
- Yang Q, Li Z, Ma H, Wang L, Martin JD (2016) Identification of the hydrogeochemical processes and assessment of groundwater quality using classic integrated geochemical methods in the South eastern part of Ordos’s basin, China. *Environ Pollut* 218:879–888. <https://doi.org/10.1016/j.envpol.2016.08.017>
- Zhang X, Li X, Gao X (2016a) Hydrochemistry and coal mining activity induced karst water quality degradation in the Niangziguan karst water system, China. *Environ Sci Pollut Res* 23(7):6286–6299. <https://doi.org/10.1007/s11356-015-5838-z>
- Zhang N, Liu B, Xiao C (2016b) Spatio-temporal variation of groundwater contamination using IEA-UEF in urban areas of Jilin City, North-eastern China. *Water Sci Technol Water Supply* J 16(5):1277–1286

Publisher’s Note Springer Nature remains neutral with regard to jurisdictional claims in published maps and institutional affiliations.